Experimental and Molecular Pathology 107 (2019) 10–22

Contents lists available at ScienceDirect

Experimental and Molecular Pathology

journal homepage: www.elsevier.com/locate/yexmp

The anti-malarial drug artesunate causes cell cycle arrest and apoptosis of triple-negative MDA-MB-468 and HER2-enriched SK-BR-3 breast cancer cells

Anna L. Greenshields[a], Wasundara Fernando[a], David W. Hoskin[a,b,c,*]

[a] Department of Pathology, Dalhousie University, Halifax, Canada
[b] Department of Microbiology and Immunology, Dalhousie University, Halifax, Canada
[c] Department of Surgery, Dalhousie University, Halifax, Canada

ARTICLE INFO

Keywords:
Artesunate
Cell cycle arrest
Cytotoxicity, Breast cancer, Reactive oxygen species

ABSTRACT

Breast cancer is the most prevalent cancer diagnosis in women, with triple-negative and human epidermal growth factor 2 (HER2)-enriched advanced breast cancers having the poorest prognoses. The morbidity and mortality associated with advanced disease, as well as the emergence of multi-drug resistant variants, highlights the urgency to develop novel therapeutic agents. Artesunate (ART) is a semi-synthetic derivative of artemisinin from the Chinese herb sweet wormwood. ART is widely used in the treatment of malaria and is well tolerated by patients. Importantly, ART also has anti-cancer activities and may therefore represent a less toxic alternative to conventional chemotherapy. In this study, we demonstrate a dose- and time-dependent inhibitory effect of ART on the growth of triple-negative MDA-MB-468 and HER2-enriched SK-BR-3 breast cancer cells, which was the result of both anti-proliferative and cytotoxic activities. ART inhibited breast cancer cell proliferation via a reactive oxygen species (ROS)-dependent G2/M arrest and ROS-independent G1 arrest. ART-treated MDA-MB-468 and SK-BR-3 cells also experienced apoptotic cell death, which was both ROS- and iron-dependent. ART-induced oxidative stress caused the loss of mitochondrial outer membrane integrity and damage to the cellular DNA of MDA-MB-468 and SK-BR-3 cells. In addition, exposure to low-dose ART sensitized MDA-MB-468 and SK-BR-3 cells to chemotherapeutic drugs. On the basis of our findings, we suggest that ART may have clinical utility in the treatment of triple-negative and HER2-enriched breast cancers.

1. Introduction

Breast cancer is the second leading cause of cancer-related death in women, who have a 1 in 8 lifetime chance of developing the disease, and was projected to kill nearly 41,000 women in the United States in 2017 (Siegel et al., 2018). The last 3 decades have seen significant improvements in the 5-year survival rate of this disease, which is currently at 90% for all stages combined; nevertheless, between 10% and 20% of breast cancer patients will suffer disease recurrence within 5 to 10 years (Brewster et al., 2008). Gene expression patterns define 5 major intrinsic subtypes of breast cancer: luminal A breast cancer, which is estrogen receptor (ER) and/or progesterone receptor (PR) positive, human epidermal growth factor receptor 2 (HER2) positive, and Ki67^{low}; luminal B breast cancer, which is ER and/or PR positive, HER2 positive or negative, and Ki67^{high}; basal-like/triple-negative breast cancer (TNBC), which is ER, PR and HER2 negative; HER2-enriched breast cancer, which is ER and PR negative but HER2 positive; and normal-like breast cancer, which is similar to luminal A disease (Dai et al., 2015). Disease prognosis is poorest for women with TNBC and HER2-enriched breast cancer. Unfortunately, current treatment options are accompanied by significant adverse side effects that negatively impact disease management (Kayl and Meyers, 2006). In addition, the development of resistance to frontline chemotherapy is a major limiting factor in breast cancer treatment, especially in the case of recurrent disease (Eckstein, 2011; Murray et al., 2012). New treatment options that are effective against chemoresistant breast cancer while causing fewer adverse side effects are therefore needed for improved management of the disease.

Artesunate (ART) is a semi-synthetic derivative of artemisinin, a lactone derived from the Chinese herb sweet wormwood (*Artemisia annua L.*), which has been used for centuries in traditional Chinese medicine; ART is currently used to treat both uncomplicated and severe malaria, including drug-resistant disease (Li and Wu, 2003). The anti-malarial bioactivity of ART, as well as artemisinin derivatives such as

* Corresponding author at: Department of Pathology, Dalhousie University, 5850 College Street, P.O. Box 15000, Halifax, Nova Scotia B3H 4R2, Canada.
E-mail address: d.w.hoskin@dal.ca (D.W. Hoskin).

https://doi.org/10.1016/j.yexmp.2019.01.006
Received 17 July 2018; Received in revised form 11 December 2018; Accepted 15 January 2019
Available online 17 January 2019
0014-4800/ © 2019 Elsevier Inc. All rights reserved.

dihydroartemisinin, is mediated through endoperoxide bridge cleavage catalyzed by free iron or heme present in the food vacuoles of *Plasmodium falciparum*, leading to reactive oxygen species (ROS) and carbon-centered radical production and alkylation of specific proteins (Shandilya et al., 2013). Artemisinin and its derivatives also exhibit antineoplastic activity (Ho et al., 2014), including in vitro cytotoxicity and tumor growth inhibition in animal models of pancreatic, ovarian, and colorectal cancer (Li et al., 2007; Du et al., 2010; Greenshields et al., 2017). Although the exact mechanism(s) that underlies the anti-cancer activities of artemisinin and its derivatives remains elusive, iron-mediated endoperoxide bridge cleavage and subsequent intracellular ROS accumulation are clearly important.

ROS are chemically-reactive oxygen-containing molecules, i.e., hydroxyl and superoxide radicals, and hydrogen peroxide, that are generated by NADPH oxidase complexes in cell membranes, peroxisomes, endoplasmic reticulum, and mitochondria (Valko et al., 2006). Iron is important in ROS generation as it catalyzes the Fenton reaction, which converts hydrogen peroxide to the highly-reactive hydroxyl radical. At low levels, ROS have an important role in the physiological processes of healthy cells; however, ROS levels that exceed the anti-oxidative capacity of the cell will cause significant oxidative damage to DNA, lipids and proteins (Valko et al., 2007). ROS-mediated lipid peroxidation damages cellular membranes and results in cell death by apoptosis or necrosis, depending on the affected site and level of damage (Ozben, 2007). Importantly, higher base-line levels of ROS in cancer cells compared to normal cells renders cancer cells more sensitive to ROS-induced cytotoxicity (Trachootham et al., 2009).

Since the widespread use of ART as an anti-malarial drug has been associated with few adverse side effects (Rosenthal, 2008), the cytotoxicity of ART against cancer cells suggests a possible use for this anti-malarial drug in the management of different cancers. In this study, we investigated the molecular basis of the anti-proliferative and cytotoxic effects of ART on MDA-MB-468 TNBC cells and SK-BR-3 HER2-enriched breast cancer cells. Our findings provide a strong rationale for the possible use of ART in breast cancer treatment.

2. Materials and methods

2.1. Reagents

ART, propidium iodide (PI), 3-(4,5-dimethylthiazol-2-yl)-2,5-diphenyltetrazolium bromide (MTT), reduced glutathione (GSH), aprotinin, bovine serum albumin (BSA), dimethyl sulfoxide (DMSO), holotransferrin (HT), leupeptin, β-mercaptoethanol, Nonidet P-40 (NP-40), pepstatin A, phenylarsine oxide, phenylmethylsulfonyl fluoride, sodium fluoride, phosphate buffered saline (PBS), sodium deoxycholate, Triton X-100, phosphatase substrate, deferiprone (DFE), *Z*-VAD-FMK, necrostatin-1, cisplatin, fluorouracil, docetaxel, 4-hydroxycyclophosphamide (4HC), doxorubicin, paclitaxel, hydrocortisone, bovine insulin, Dulbecco's Modified Eagle's Medium (DMEM), and F12 medium were all purchased from Sigma-Aldrich Canada (Oakville, ON). DNase-free RNase A was purchased from Qiagen Inc. (Mississauga, ON). Cell Trace™ Oregon Green 488 and 5-(and-6)-chloromethyl-2′,7′-dichlorodihydrofluorescein diacetate, acetyl ester (CM-H_2DCFDA) were purchased from Molecular Probes (Eugene, OR, USA). Annexin-V-FLUOS was purchased from Roche Diagnostics (Laval, QC). Protein assay dye reagent concentrate was purchased from BioRad (Hercules, CA). Fetal bovine serum (FBS), horse serum, L-glutamine, 10,000 units/ml penicillin/10,000 μg/ml streptomycin, 4-(2-hydroxyethyl)-1-piperazineethanesulfonic acid (HEPES) buffer solution, and 0.25% trypsin-EDTA, were purchased from Invitrogen Canada Inc. (Burlington, ON). Sodium orthovanadate was purchased from EMD Chemicals, Inc. (Gibbstown, NJ). Ethylene diamine tetraacetic acid (EDTA) was purchased from EM 46 Industries Inc. (Hawthorne, NY). Dithiothreitol, ethylene glycol tetraacetic acid (EGTA), paraformaldehyde, sodium dodecyl sulfate (SDS), Tris base, and Tween-20 were purchased from Bio-Shop Canada Inc. (Burlington, ON). Human epidermal growth factor and basic fibroblast growth factor were from Peprotech (Montreal, QC). Luminata™ Forte Western HRP Substrate was purchased from Millipore (Billerica, MA). A 100 μM stock of ART dissolved in DMSO was stored in aliquots at −20 °C until use.

2.2. Antibodies

Mouse anti-p21 monoclonal antibody (mAb), rabbit anti-phospho-Chk2 (Thr68) polyclonal antibody (Ab), mouse anti-cyclin D3 mAb, mouse anti-CDK4 mAb, mouse anti-retinoblastoma protein (Rb) mAb, and rabbit anti-γH2AX mAb were purchased from Cell Signaling Technology Inc. (Beverly, MA). Mouse anti-poly(ADP-ribose) polymerase-1 (PARP-1) mAb, bovine anti-goat IgG Ab coupled to horse radish peroxidase (HRP), goat anti-mouse IgG-HRP Ab, donkey anti-rabbit IgG-HRP Ab, and goat anti-actin Ab were from Santa Cruz Biotechnology (Santa Cruz, CA). Mouse anti-cyclin B1 mAb, rabbit anti-CDK1 Ab, mouse anti-CDK4 mAb, mouse anti-CDC25C mAb, mouse anti-cyclin A mAb, and mouse anti-E2F-1 mAb were purchased from Millipore. Rabbit anti-second mitochondria-derived activator of caspases (SMAC) mAb was from Epitomics (Burlingame, CA). Mouse anti-cytochrome *c* mAb was purchased from BD Biosciences (Mississauga, ON).

2.3. Cell lines

SK-BR-3 breast cancer cells were kindly provided by Dr. G. Dellaire (Dalhousie University, Halifax, NS). MDA-MB-468 breast cancer cells were a gift from Dr. P. Lee (Dalhousie University). Native MCF-7 and MCF-7-derived TX400 breast cancer cells were a generous gift from Dr. K. Goralski (Dalhousie University). MDA-MB-231 human breast cancer cells were generously provided by Dr. S. Drover (Memorial University of Newfoundland, St John's, NL). T47D human breast cancer cells were a gift from Dr. J. Blay (University of Waterloo, Waterloo, ON). All breast cancer cell lines were grown in DMEM supplemented with 10% heat-inactivated (56 °C for 30 min) FBS, 2 mM L-glutamine, 5 mM HEPES buffer (pH 7.4), 100 U/ml penicillin, and 100 μg/ml streptomycin; henceforth, referred to as complete DMEM (cDMEM). TX400 MCF-7 cell medium was supplemented with 400 ng/ml paclitaxel to maintain drug resistance; cells were cultured for one passage without paclitaxel prior to use in experiments. All breast cancer cell lines were maintained at 37 °C in 10% CO_2 humidified atmosphere. MCF-10A normal mammary epithelial cells were obtained from Dr. Paola Marcato (Dalhousie University) and cultured at 37 °C in a humidified 5% CO_2 atmosphere incubator using F12/DMEM (1,1) medium supplemented with 10% horse serum, 0.02 μg/ml epidermal growth factor, 0.5 μg/ml hydrocortisone, 10 μg/ml bovine insulin, 100 U/ml penicillin and 100 μg/ml streptomycin.

2.4. Breast cancer spheroids

MCF-7 cells in F12 medium supplemented with 20 ng/ml basic fibroblast growth factor, 20 ng/ml epidermal growth factor, 100 U/ml penicillin, 100 μg/ml streptomycin and 1 × B27 serum-free supplement were seeded at 3×10^4 cells/well into ultra-low attachment Costar 6-well plates and cultured at 37 °C in a 10% CO_2 humidified atmosphere for 7 days in order to allow spheroid development. Cultures were fed with fully supplemented fresh medium every 72 h.

2.5. MTT assay

Mitochondrial succinate dehydrogenase activity, as determined by MTT assay, was used to assess the growth of MCF-10A and breast cancer cell lines. Cells were seeded at 5×10^3 cells/well into 96-well plates and cultured for 24, 48, or 72 h in the absence or presence of increasing concentrations of ART. In one set of experiments, breast cancer cells

were pretreated with 10 μM HT or vehicle for 1 h at 37 °C, and then HT-containing medium was removed and replaced with DMSO vehicle- or ART-containing medium. In another set of experiments, breast cancer cell cultures were treated with ART or DMSO vehicle for 1 h at 37 °C prior to culture for 72 h in the absence or presence of increasing concentrations of 4HC, cisplatin, doxorubicin, FU, or docetaxel. MTT was added to cultures to a final concentration of 0.5 μg/ml 2 h prior to termination of culture. Plates were centrifuged at 1400*g* for 5 min, supernatant was discarded and formazan crystals were solubilised in 100 μl DMSO. Changes in well optical density were determined at 490 nm using an Asys Expert 96 Microplate Reader from Biochrom (Cambridge, UK). Changes in the % decrease in viable cell number are shown relative to the medium control.

2.6. Acid phosphatase assay

Total cellular acid phosphatase activity was used to compare the viability of control and ART-treated MCF-7 breast cancer spheroids, as well as control and ART-treated TX400 MCF-7 and MCF-7 cells since P-glycoprotein in TX400 MCF-7 cells precluded the use of an MTT assay (Vellonen et al., 2004). MCF-7 and TX400 MCF-7 cells were seeded at 5×10^3 cells/well into 96-well plates and cultured in the absence or presence of ART for 48 or 72 h. MCF-7 breast cancer spheroids were cultured for 72 h in the absence or presence of ART. At the end of culture, cells or breast cancer spheroids were washed in PBS, re-suspended in 200 μl or 1 ml phosphatase assay buffer (0.1 M sodium acetate pH 5.5, 1 μl/ml Triton X-100 and 4 mg/ml phosphatase substrate) diluted 1:1 in PBS, respectively, and incubated for 90 min in the dark at 37 °C. The reaction was stopped with 1 N NaOH at a final dilution of 1:20 and OD was determined at 405 nm using an Asys Expert 96 Microplate Reader. Changes in the % decrease in total cellular acid phosphatase activity are shown relative to the medium control.

2.7. Colony formation assay

A clonogenic assay was used to determine the effect of ART on the ability of single MDA-MB-468 breast cancer cells to form colonies. Cells in T75 flasks were cultured for 24 h in the absence or presence of increasing concentrations of ART, and then viable cells were harvested, washed with PBS, and counted. In one set of experiments, cells were cultured for 24 h in the absence or presence of 0.1 μM cisplatin without or with 5 μM ART. Equal numbers of cancer cells were serially diluted in fresh cDMEM, plated into 6-well plates in triplicate at 2×10^3, 1×10^3, 5×10^2, or 2.5×10^2 cells/well, and cultured for 13–14 days to allow colony formation. Colonies were washed with PBS, fixed and stained with 0.4% crystal violet in methanol for 10 min, and then washed with water. Only colonies containing > 50 cells were counted. The plating efficiency (PE) and surviving fraction (SF) (%) were calculated as follows:

PE = #of colonies formed in the medium control/#of cells seeded

SF = (#of colonies formed after treatment/(#of cells seeded* PE))*100

2.8. Cell proliferation assay

MDA-MB-468 or SK-BR-3 breast cancer cells were seeded into 6-well plates at 5×10^4 cells/well, allowed to adhere overnight, and stained for 45 min with 1.25 μM Cell Trace™ Oregon Green 488 dye. Cells were washed with cDMEM, and then allowed to recover for 2–3 h. Some cultures were harvested, fixed in 1% paraformaldehyde and stored at 4 °C to serve as baseline staining controls. The remaining cultures were treated for 72 h with medium, DMSO vehicle, or 25 or 50 μM ART. Some cultures received 10 mM GSH 30 min prior to the addition of ART to determine the impact of ROS removal on the effect of ART on breast cancer cell proliferation. The number of cell divisions (n) was calculated using the mean channel fluorescence (MCF) of the sample (MCF_{sample}) and the MCF of the baseline control ($MCF_{baseline}$) as follows: $MCF_{baseline} = (2^n)(MCF_{sample})$.

2.9. Cell cycle analysis

MDA-MB-468 and SK-BR-3 breast cancer cells were serum-starved for up to 24 h for G0 synchronization. Cells were then seeded into 6-well plates at 5×10^4 cells/well, allowed to adhere overnight, and cultured for 48 h in the absence or presence of ART. Some cultures received 10 mM GSH 30 min prior to the addition of ART to determine the impact of ROS removal on the effect of ART on cell cycle progression. At the end of culture cells were harvested, washed in cold PBS and resuspended in 0.5 ml cold PBS to which ice-cold 70% ethanol was then added dropwise to a final volume of 5 ml with constant agitation. Samples were stored at −20 °C for a minimum of 24 h, and then washed with PBS and resuspended in PI solution (0.1% *v*/v Triton X-100 in PBS containing 0.2 mg/ml DNase-free RNase A and 0.02 mg/ml PI), incubated for 30 min at room temperature, and analyzed by flow cytometry on a FACSCalibur flow cytometer using Becton Dickinson (BD) CellQuest™ software (version 3.3; BD Biosciences, Mississauga, ON). The DNA content of single, live cells was analyzed using ModFit LT 3.0 (Verity Software House, Topsham ME).

2.10. Western blot analysis

Following the desired treatments in T75 flasks, MDA-MB-468 and SK-BR-3 breast cancer cells were harvested, washed with cold PBS, and lysed on ice for 30 min in 50 μl RIPA lysis buffer (1% NP-40, 0.5% sodium deoxycholate, 0.1% SDS, 20 mM Tris, 150 mM NaCl, 1 mM EDTA, 1 mM EGTA at pH 7.5 with 5 μg/ml leupeptin, 5 μg/ml pepstatin, 10 μg/ml apotinin, 100 μM sodium orthovanadate, 1 mM dithiothreitol, 10 mM sodium fluoride, 10 μM phenylarsine oxide and 1 mM phenylmethylsulfonyl fluoride). Lysates were clarified by centrifugation at 14,000*g* at 4 °C for 10 min and protein concentration of cell lysates was determined using Bio-Rad protein assay dye as per the manufacturer's instructions. For isolation of the cytosolic fraction, cells were lysed on ice for 15 min in 50 μl digitonin lysis buffer (75 mM NaCl, 1 mM NaH_2PO_4, 8 mM Na_2HPO_4, 250 mM sucrose and 190 μg/ml digitonin with 5 μg/ml leupeptin, 5 μg/ml pepstatin, 10 μg/ml apotinin, 100 μM sodium orthovanadate, 1 mM dithiothreitol, 10 mM sodium fluoride and 10 μM phenylarsine oxide). Samples were centrifuged at 1000*g* at 4 °C for 5 min to remove intact cells. Lysates were then clarified by centrifugation at 14,000*g* at 4 °C for 10 min and the protein concentration of the lysates was determined using Bio-Rad protein assay dye. Equal amounts of protein were resolved on 15, 12, or 7.5% SDS-polyacrylamide gels (depending on desired protein size) for 1 h at 200 V, and then protein bands were transferred onto a nitrocellulose membrane using the iBlot transfer system (Invitrogen) as per the manufacturer's instructions. Membranes were blocked for 1 h or overnight in Tris-buffered saline (200 mM Tris, 1.5 M NaCl; pH 7.6) containing 0.05% Tween-20 (T-TBS) with 5% w/v skim milk powder, and then washed in T-TBS and incubated overnight at 4 °C with an optimal dilution of primary Ab in either 5% w/v skim milk powder in T-TBS or 5% BSA in T-TBS, depending on the manufacturer's recommendation. After additional washes in T-TBS, blots were incubated overnight at 4 °C or for 1 h at room temperature with an optimal dilution of the appropriate secondary Ab in 5% w/v skim milk powder in T-TBS. Blots were washed and protein bands were visualized using Luminata™ Forte western HRP substrate and film exposure. To confirm even protein loading, blots were reprobed with goat anti-actin Ab.

2.11. Flow cytometric measurement of cell death

MDA-MB-468 breast cancer cells, SK-BR-3 breast cancer cells, or MCF-10A normal mammary epithelial cells were seeded into 6-well

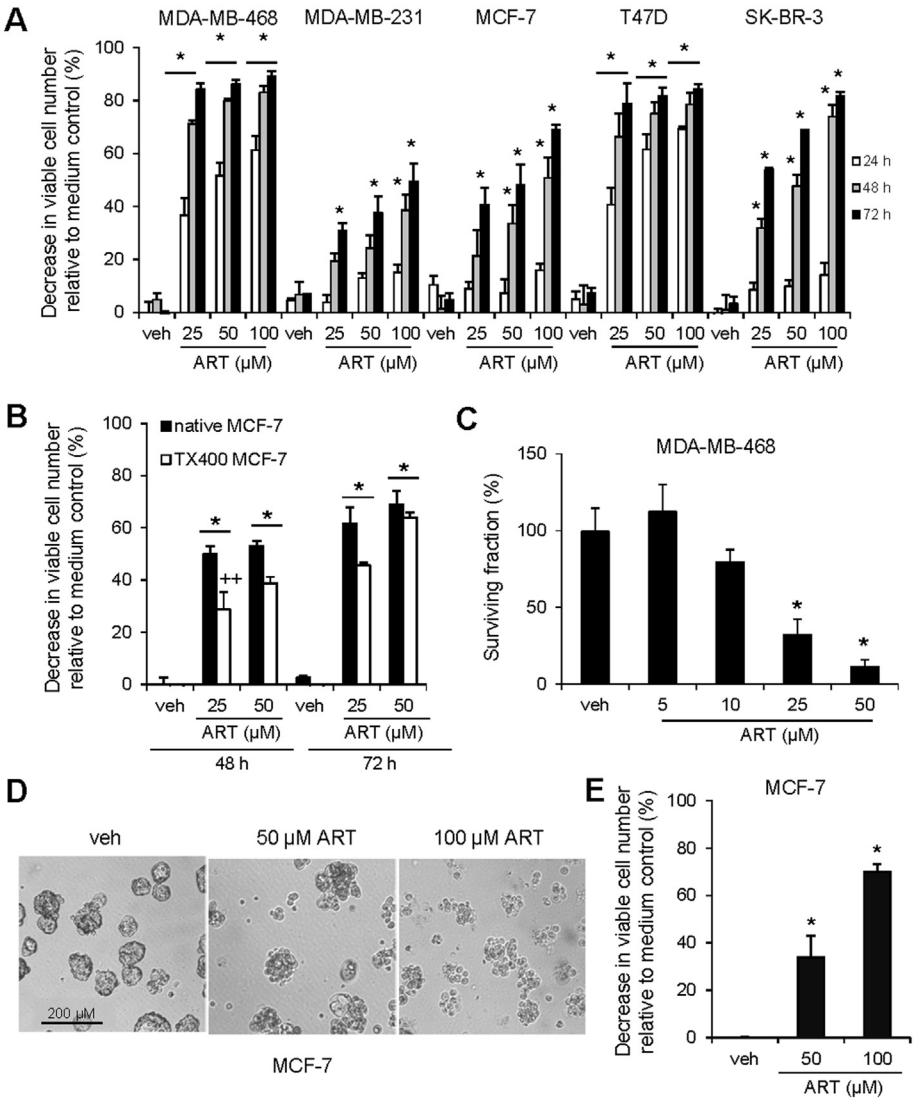

Fig. 1. ART inhibits breast cancer cell growth. (A) MDA-MB-468, MDA-MB-231, MCF-7, T47D, and SK-BR-3 breast cancer cells were cultured in the presence of the indicated concentrations of ART or vehicle (veh) for the specified times. Changes in viable cell number were determined using an MTT assay. (B) Parental MCF-7 or paclitaxel-resistant TX400 MCF-7 breast cancer cells were cultured in the presence of the indicated concentrations of ART or vehicle (veh) for the specified times. Changes in viable cell number were determined using an acid phosphatase assay. (C) MDA-MB-468 breast cancer cells were cultured in the presence of the indicated concentrations of ART or vehicle (veh) for 24 h, and then equal numbers of viable cells were serially diluted and seeded in triplicate into 6-well plates. Following ~14 d culture, colonies were stained with crystal violet and counted. (D, E) MCF-7 spheroids were cultured in the presence of the indicated concentrations of ART or vehicle (veh) for 72 h, and then spheroids were photographed and changes in viable cell number were determined using an acid phosphatase assay. (A, B, C, E) Data shown are the mean of at least 3 independent experiments ± SEM; $^*p < .05$ compared to the vehicle control, determined by one-way ANOVA with Tukey-Kramer post-test.

plates at 5×10^4 cells/well and cultured for 24, 48 or 72 h in the absence or presence of ART. Some cultures were pretreated with 10 μM HT or vehicle for 1 h, then HT was removed and replaced with ART or DMSO vehicle to determine the impact of increased iron levels on the cytotoxic effect of ART. In other experiments, cultures received medium, 12.5 μg/ml DFE, or 10 mM GSH 30 min before the addition of ART or DMSO vehicle to determine the impact of iron withdrawal (DFE) or ROS removal (GSH) on killing by ART. To explore the role of caspases and necroptosis in ART-induced cytotoxicity, cultures received 50 μM *Z*-VAD-FMK or 40 μM necrostatin-1, respectively, 1 h prior to culture in the presence or absence of ART. Control cultures were treated with DMSO vehicle. The requirement of oxygen for ART-induced cytotoxicity was determined by culturing cells in the absence or presence of ART in a normoxic or hypoxic environment (0.5% O_2; C-Chamber Hypoxic Unit, BioSpherix, Lacona, NY). Some ART-treated cultures were exposed to a normoxic environment for 24 h and then transferred to a hypoxic environment for an additional 24 h. Following culture, non-adherent and adherent cells were pooled and washed with PBS, then stained with Annexin V-FLUOS (diluted as per the manufacturer's instructions) and PI (1 μg/ml) in 50 μl detection buffer (10 mM HEPES, 140 mM NaCl, and 5 mM $CaCl_2$) for 15 min at room temperature. After additional washes cells were resuspended in detection buffer, and early and late apoptotic/necrotic cell death was measured with a FACSCalibur flow cytometer using BD CellQuest™ software (version 3.3). Data were analyzed using FCS Express software (version 3.0; De Novo Software, Thornhill, ON). Early apoptosis (%) is the percentage of cells which stain positive for Annexin-V-FLUOS and negative for PI. Late apoptosis/necrosis (%) is the percentage of cells which stain positive for both Annexin-V-FLUOS and PI.

2.12. Caspase activation assay

MDA-MB-468 or SK-BR-3 breast cancer cells were seeded into 6-well plates at 5×10^4 cells/well, allowed to adhere overnight, and then cultured for 48 h in the absence or presence of ART. At the end of culture, adherent and nonadherent cells were pooled and stained for 1 h at 37 °C with the fluorescent inhibitor of caspases (FLICA) reagent, as per the manufacturer's instructions (Vybrant® FAM Poly Caspases Assay Kit, Invitrogen). Stained cells were washed as per the manufacturer's directions and fluorescence was determined by flow cytometry as previously described.

2.13. Flow cytometric determination of mitochondrial outer membrane integrity

MDA-MB-468 or SK-BR-3 breast cancer cells were seeded into 6-well plates at 5×10^4 cells/well, allowed to adhere overnight, and cultured in the absence or presence of increasing concentrations of ART for 24,

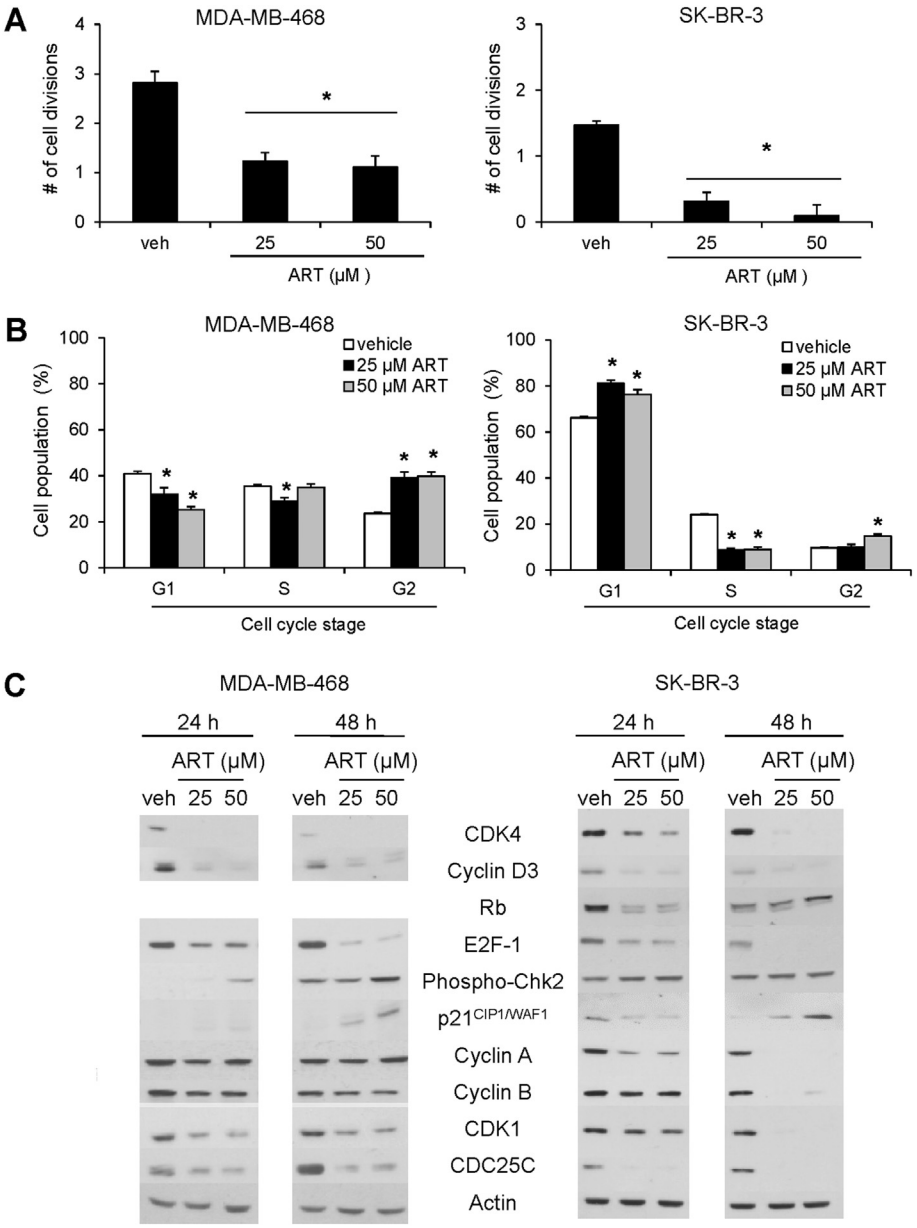

Fig. 2. ART inhibits breast cancer cell proliferation and induces cell cycle arrest. (A) MDA-MB-468 and SK-BR-3 breast cancer cells were stained with Oregon Green 488 dye and cultured for 72 h in the presence of the indicated concentrations of ART or vehicle (veh). Cell division number, as indicated by altered fluorescence intensity, was determined by flow cytometry. (B) MDA-MB-468 and SK-BR-3 cells were cultured for 48 h in the presence of the indicated concentrations of ART or vehicle. Cells were then permeabilized, fixed in ethanol, and stored at −20 °C for at least 24 h prior to staining with PI for measurement of DNA content by flow cytometry. (A, B) Data shown are the mean of at least 3 independent experiments ± SEM; $*p < .05$ compared to respective vehicle controls, determined by a one-way ANOVA with a Tukey-Kramer post-test. (C) MDA-MB-468 and SK-BR-3 breast cancer cells were treated with the indicated concentrations of ART or vehicle (veh) for 24 or 48 h. Cells were lysed and total protein was collected for western blot analysis of cell cycle proteins. Results representative of 3 independent experiments are shown.

48, or 72 h. Some cultures received 10 mM GSH 30 min before the addition of ART or DMSO vehicle to determine the effect of ROS removal (GSH) on mitochondrial outer membrane integrity. Adherent and nonadherent cells were pooled and stained for 15 min at room temperature with 40 nM $DiOC_6$ in cDMEM for analysis by flow cytometry as previously described.

2.14. Flow cytometric detection of intracellular ROS accumulation

MDA-MB-468 or SK-BR-3 breast cancer cells were seeded into 6-well plates at 1×10^5 cells/well and allowed to adhere overnight. The cell monolayer was washed with warm PBS and then stained for 30 min in the dark with 5 μM CM-H_2DCFDA in phenol-red- and serum-free cDMEM. Following an additional wash with warm PBS, cDMEM containing 1% heat-inactivated FBS was added to the wells. Cells were cultured for 8 or 24 h in the absence or presence of ART. As a negative control, some cultures were pretreated with 10 mM GSH for 30 min prior to ART treatment. To determine the effect of elevated iron levels on ART-induced ROS accumulation, other cultures were pretreated with 10 μM HT for 1 h, then HT was removed and cells were treated with ART or DMSO vehicle. At the end of culture, adherent and nonadherent cells were pooled and resuspended in ice-cold PBS for analysis by flow cytometry as previously described. Background autofluorescence of ART-treated cells was subtracted from the fluorescence of CM-H_2DCFDA-stained cells. Intracellular ROS accumulation relative to the medium control was calculated using the following formula: MCF_{sample} - AUTO/$MCF_{medium} \times 100$, where MCF_{sample} is the mean channel fluorescence of the sample, AUTO is the auto-fluorescence of ART and MCF_{medium} is the mean channel fluorescence of the medium control.

2.15. Statistical analysis

GraphPad InStat (GraphPad Software Inc., version 3.0) was used to test statistical significance ($p < .05$) by Student's *t*-test or one-way analysis of variance (ANOVA) with Tukey multiple comparisons post-test, as appropriate.

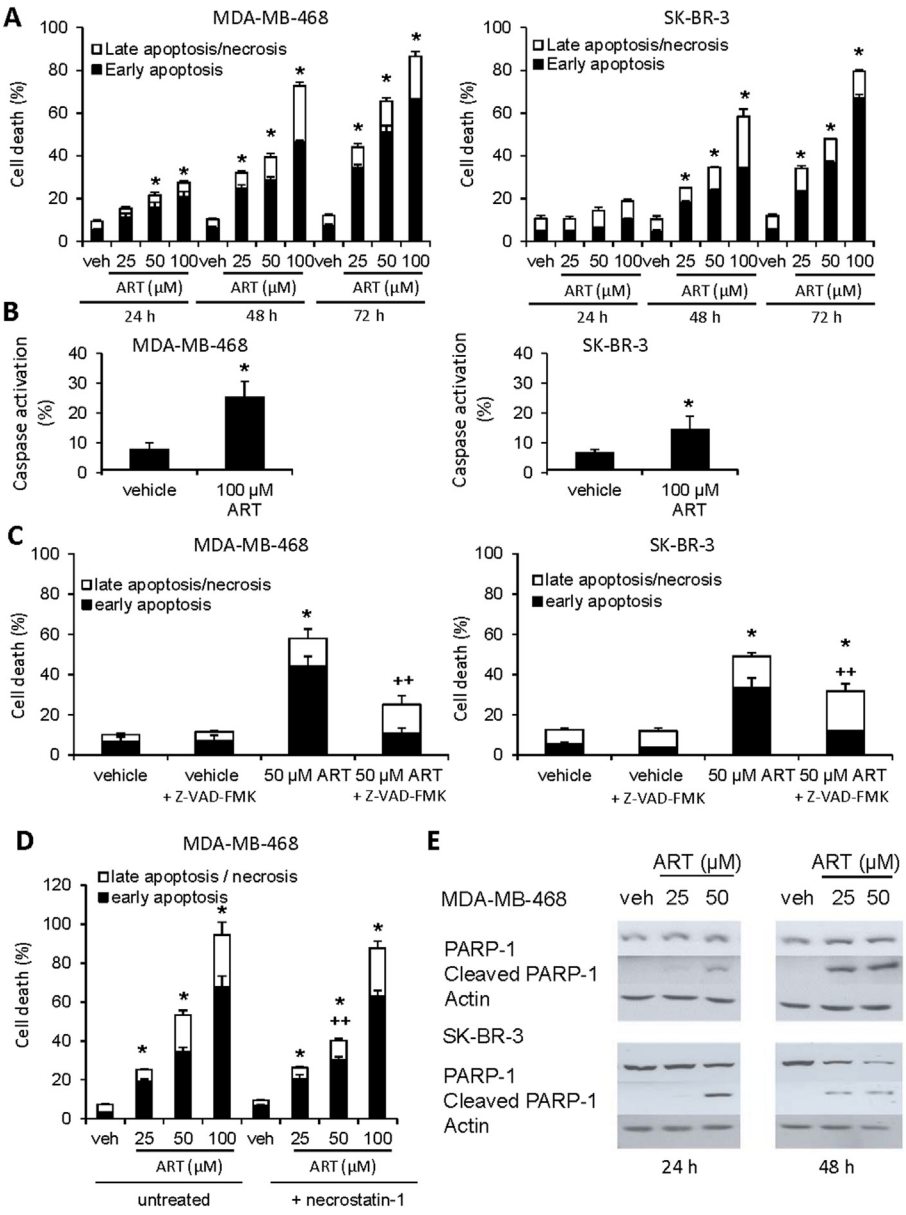

Fig. 3. ART induces apoptosis of breast cancer cells. (A) MDA-MB-468 and SK-BR-3 breast cancer cells were cultured for the indicated times in the presence of the specified concentrations of ART or vehicle (veh), and then stained with Annexin-V-FLUOS/PI for flow cytometric analysis. (B) MDA-MB-468 and SK-BR-3 breast cancer cells were cultured for 24 h or 48 h, respectively, in the presence of 100 μM ART or vehicle, and then stained with FLICA for flow cytometric analysis. (C, D) MDA-MB-468 and SK-BR-3 cells were cultured for 72 h in the presence of 50 μM ART or vehicle without or with (C) 50 μM *Z*-VAD-FMK, or (D) 40 μM necrostatin-1. Cells were then stained with Annexin-V-FLUOS/PI for flow cytometric analysis. (A, C, D) Data shown are the mean of at least 3 independent experiments ± SEM; $^{*}p < .05$ compared to the vehicle control, determined by a one-way ANOVA with a Tukey-Kramer post-test; $^{++}p < .05$ compared to total cell death in the absence of Z-VAD-FMK or necrostatin-1, determined by a one-way ANOVA with a Tukey-Kramer post-test. (E) MDA-MB-468 and SK-BR-3 cells were cultured for 24 or 48 h in the presence of the indicated concentrations of ART or vehicle (veh). Cells were then lysed and total protein collected for western blot analysis of intact and cleaved PARP-1. Blots showing cleaved PARP-1 are longer exposures than those showing intact PARP-1 in order to permit adequate band detection. Actin expression was used to confirm equal protein loading. Results from a representative experiment ($n = 3$) are shown.

3. Results

3.1. ART inhibits breast cancer cell growth

MTT assays were used to determine the effect of ART on the growth of 5 different breast cancer cell lines: MCF-7 (ER-positive, caspase 3-negative, p53-wildtype), MDA-MB-468 (ER-negative, PR-negative, HER2-negative, Rb-null, p53-mutant), MDA-MB-231 (ER-negative, PR-negative, HER2-negative, p53-mutant), T47D (ER-positive, p53-mutant), and SK-BR-3 (ER-negative, p53-mutant, HER2–positive). ART had a significant dose- and time-dependent inhibitory effect on the growth of all 5 breast cancer cell lines tested (Fig. 1A); MDA-MB-468 > T47D > SK-BR-3 > MCF-7 > MDA-MB-231. In addition, paclitaxel-resistant TX400 MCF-7 (ER-positive) cells, a variant of the MCF-7 line that over-expresses P-glycoprotein, exhibited a significant reduction in growth when treated with ART (Fig. 1B); unfortunately, paclitaxel-resistant triple-negative (MDA-MB-231 or MDA-MB 468) cells and paclitaxel-resistant HER2-positive (SK-BR-3) cells were not available for use in our study. ART also suppressed the growth of MCF-10A normal mammary epithelial cells (Supplemental Fig. 1), albeit to a lesser extent in all but one of the breast cancer cell lines. We next used a clonogenic assay to evaluate the effect of ART on the colony-forming capacity of MDA-MB-468 cells. Prior exposure to 25 and 50 μM concentrations of ART for 24 h had a significant inhibitory effect on colony formation by surviving cells (Fig. 1C). We also examined the effect of ART on spheroid formation by MCF-7 breast cancer cells. In our hands, and consistent with a recent report by Froehlich et al. (2016), MCF-7 (ER-positive) cells routinely formed large well-defined multicellular spheroids, unlike MDA-MB-231 or MDA-MB-468 (triple-negative) cells, while SK-BR-3 (HER2-positive) cells did not form spheroids. MCF-7 spheroids grown in the presence of ART were smaller, less compact and irregular in shape compared to controls; numerous single floating cells with the morphology of dead or dying cells were also present (Fig. 1D). In addition, acid phosphatase assays showed a substantial decrease in the number of viable MCF-7 cells within ART-treated spheroids relative to vehicle-treated controls (Fig. 1E). Collectively, these findings indicate that ART inhibited breast cancer cell growth in both 2- and 3-dimensional culture systems. MDA-MB-468 and SK-BR-3 cells were used in subsequent experiments since these breast cancer cell lines were among the most sensitive to ART-mediated growth inhibition.

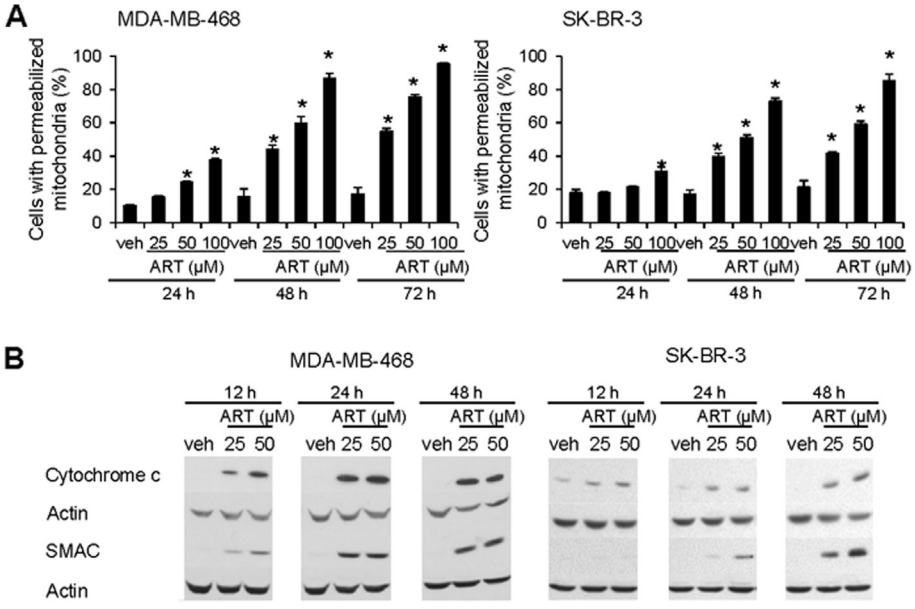

Fig. 4. ART-induced apoptosis of breast cancer cells is associated with loss of mitochondrial membrane integrity and the release of mitochondrial cytochrome *c* and SMAC. (A) MDA-MB-468 and SK-BR-3 breast cancer cells were cultured for the indicated times in the presence of the specified concentrations of ART or vehicle (veh), and then stained with $DiOC_6$ for flow cytometric analysis. Data shown are the mean of at least 3 independent experiments ± SEM; $^{*}p < .05$ compared to the vehicle control, determined by a one-way ANOVA with a Tukey-Kramer post-test. (B) MDA-MB-468 and SK-BR-3 cells were cultured for 12, 24 or 48 h in the presence of the indicated concentrations of ART or vehicle (veh). Cells were then lysed and proteins in the cytoplasmic fraction were collected for western blot analysis of cytochrome *c* and SMAC content. Actin expression was used to confirm equal protein loading. Results from a representative experiment (n = 3) are shown.

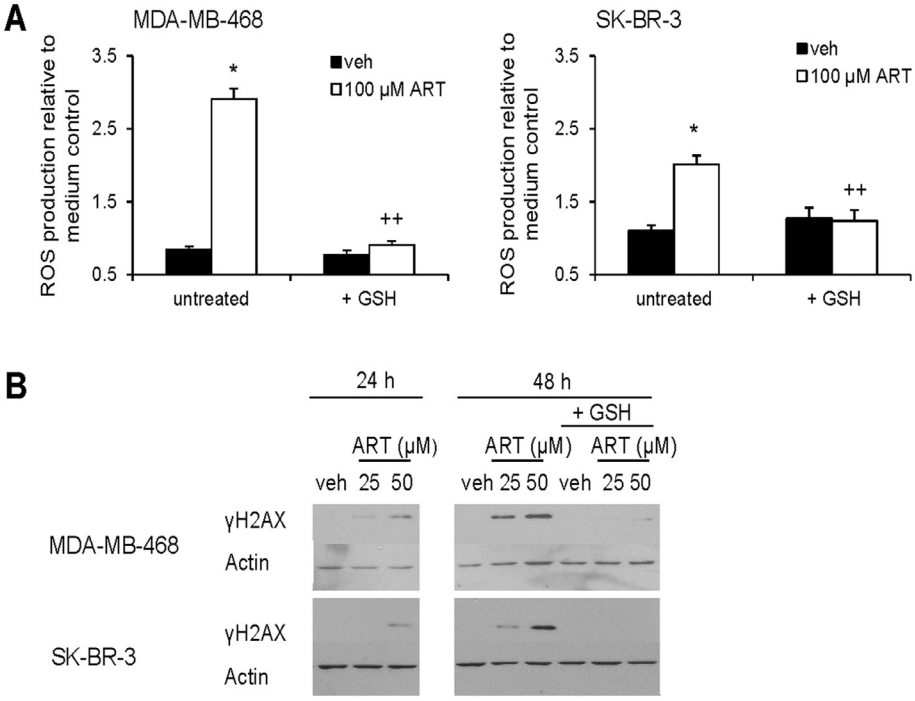

Fig. 5. ART-induced ROS causes DNA damage in breast cancer cells. (A) MDA-MB-468 and SK-BR-3 breast cancer cells were stained with CM-H_2DCFDA, then cultured for 24 h in the presence of 100 μM ART or vehicle (veh) without or with GSH. ROS accumulation was determined by flow cytometry. Data shown are the mean relative ROS production of at least 3 independent experiments ± SEM; * $p < .05$ compared to the vehicle, $^{++}$ $p < .05$ compared to treatment without 10 mM GSH, determined by a one-way ANOVA with a Tukey-Kramer post-test. ART background fluorescence was subtracted from all values. (B) MDA-MB-468 and SK-BR-3 cells were cultured for 24 or 48 h in the presence of the indicated concentrations of ART or vehicle (veh). Cells were then lysed and total protein was collected for western blot analysis of γH2AX levels. Actin expression was used to confirm equal protein loading. Results from a representative experiment (n = 3) are shown.

3.2. ART induces cell cycle arrest in MDA-MB-468 and SK-BR-3 breast cancer cells

MDA-MB-468 and SK-BR-3 breast cancer cells were stained with Oregon Green 488 dye to determine the effect of ART on cell division. As shown in Fig. 2A, ART-treated breast cancer cells went through significantly fewer cycles of division than control cells treated with vehicle alone. Cell cycle analysis revealed that ART-treated MDA-MB-468 cells displayed a marked increase in the fraction of cells present in the G2/M phase of the cell cycle compared to control cells (Fig. 2B). SK-BR-3 cells arrested in the G1 phase; however, there was also a significant increase in the fraction of cells in G2/M following treatment with 50 μM ART. In addition, there was a dose-dependent accumulation of ART-treated MDA-MB-468 and SK-BR-3 cells in the sub-G1 fraction (Supplemental Fig. 2), which suggested that some ART-treated breast cancer cells were undergoing apoptosis. Western blot analysis revealed changes in the expression of key cell cycle regulatory proteins as a result of exposure to ART. Fig. 2C shows that ART affected the expression of regulatory proteins involved in all stages of the cell cycle, in the majority of cases being most evident 48 h after exposure to ART. E2F-1, cyclin D3, CDC25C, CDK1, and CDK4, expression was decreased and $p21^{CIP1/WAF1}$ expression was increased in ART-treated MDA-MB-468 and SK-BR-3 cells. Expression of cyclin A and cyclin B was also decreased in ART-treated SK-BR-3 cells, whereas there was little effect on these proteins in MDA-MB-468 cells. On the other hand, ART treatment caused phospho-Chk2 expression to increase in MDA-MB-468 cells but not in SK-BR-3 cells. In addition, a transitory decrease in Rb expression was observed in ART-treated SK-BR-3 cells; Rb expression was not assessed in Rb-negative MDA-MB-468 cells. Taken together, these data indicate an anti-proliferative effect of ART on TNBC cells and HER2-

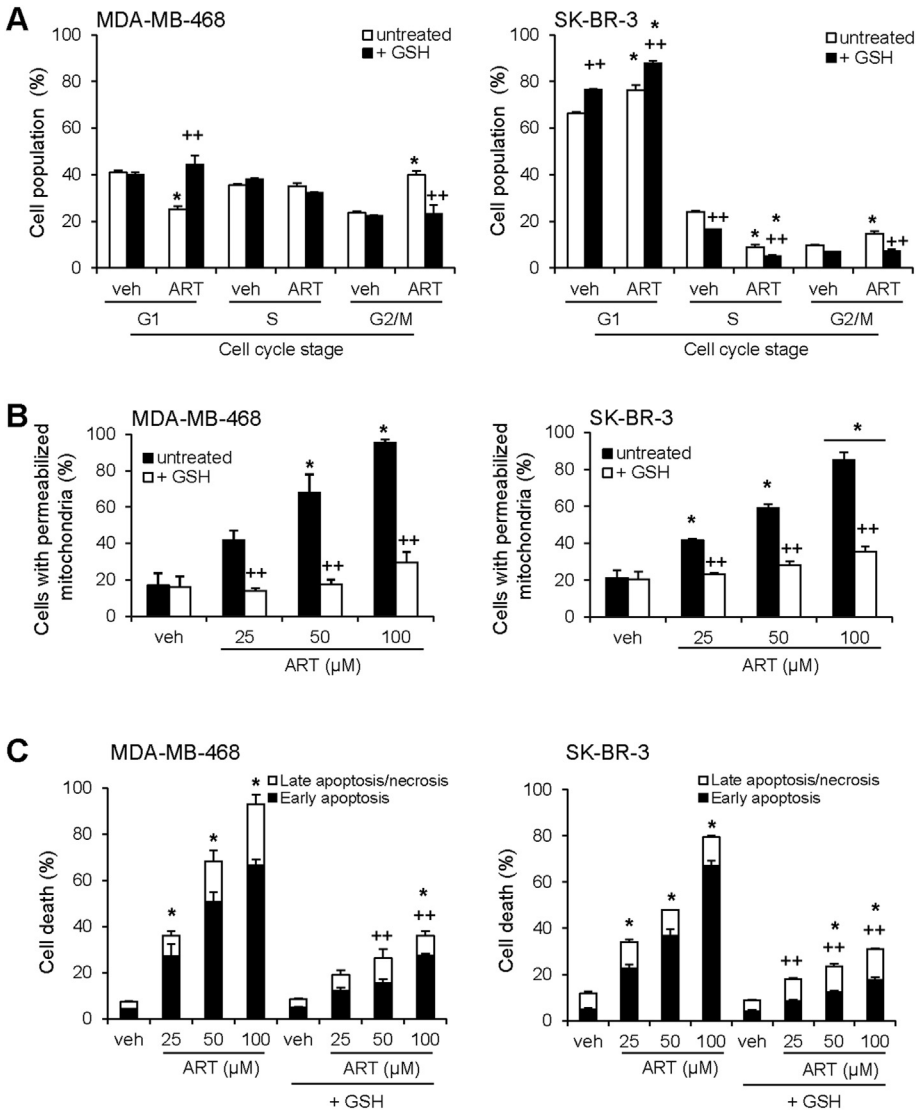

Fig. 6. ART-induced ROS contributes to cell cycle alterations, mitochondrial membrane permeabilization, and apoptosis induction. (A) MDA-MB-468 and SK-BR-3 breast cancer cells were cultured for 48 h in the presence of 50 μM ART or vehicle (veh) without or with 10 mM GSH. Cells were then permeabilized, fixed in ethanol, and stored at −20 °C for at least 24 h prior to staining with PI for measurement of DNA content by flow cytometry. (B) MDA-MB-468 and SK-BR-3 cells were cultured for 72 h in the presence of the indicated concentrations of ART or vehicle (veh) without or with 10 mM GSH. Cells were then stained with $DiOC_6$ and analyzed by flow cytometry. (C) MDA-MB-468 and SK-BR-3 cells were cultured for 72 h in the presence of the indicated concentrations of ART or vehicle (veh) without or with 10 mM GSH. Cells were then stained with Annexin-V-FLUOS/PI for flow cytometric analysis. (A, B, C) Data shown are the mean of at least 3 independent experiments ± SEM; $^{*}p < .05$ compared to the appropriate vehicle control; $^{++}$ $p < .05$ compared to treatment in the absence of GSH, determined by a one-way ANOVA with a Tukey-Kramer post-test.

enriched breast cancer cells.

3.3. ART triggers apoptosis in MDA-MB-468 and SK-BR-3 breast cancer cells

The capacity of ART to kill breast cancer cells was determined by flow cytometric analysis of MDA-MB-468 and SK-BR-3 cells stained with Annexin-V-FLUOS/PI following culture in the absence or presence of ART. As shown in Fig. 3A, ART-treated MDA-MB-468 and SK-BR-3 cells exhibited a dose- and time-dependent increase in the fraction of cells undergoing early apoptosis (indicated by an increase in Annexin-V-FLUOS staining), as well as a smaller percentage of late apoptotic/necrotic cells (indicated by staining with both Annexin-V-FLUOS and PI), compared to the vehicle control. In contrast, MCF-10A normal mammary epithelial cells that were treated with ART showed no significant loss of viability relative to the vehicle control (Supplemental Fig. 3). ART treatment induced caspase activity in both MDA-MB-468 and SK-BR-3 cells (Fig. 3B), and inclusion of the pan-caspase inhibitor *Z*-VAD-fmk reduced the cytotoxic effect of ART on breast cancer cells (Fig. 3C), indicating the involvement apoptosis-associated caspases in ART-induced cell death. However, the pan-caspase inhibitor Z-VAD-fmk was not able to completely prevent ART-induced cytotoxicity, suggesting the contribution of one or more caspase-independent cell death processes. The receptor-interacting protein kinase 1 (RIP1) inhibitor, necrostatin-1, did not substantially improve the viability of ART-treated MDA-MB-468 cells (Fig. 3D), implying that ART did not kill breast cancer cells via necroptosis. Consistent with caspase-dependent apoptosis, PARP-1 was cleaved in ART-treated SK-BR-3 and MDA-MB-468 cells (Fig. 3E). To further investigate the mechanism by which ART triggered the apoptotic death of breast cancer cells, ART-treated MDA-MB-468 and SK-BR-3 cells were stained with the mitochondrial dye $DiOC_6$ to determine whether ART affected mitochondrial outer membrane integrity. As shown in Fig. 4, exposure to ART resulted in both breast cancer cell lines showing a time- and dose-dependent increase in mitochondrial outer membrane permeability (Fig. 4A) that was accompanied by the release of cytochrome *c* and SMAC from mitochondria into the cytosolic compartment (Fig. 4B). These findings are consistent with ART-mediated induction of the intrinsic pathway of apoptosis.

3.4. ART induces ROS-dependent DNA damage in MDA-MB-468 and SK-BR-3 breast cancer cells

CM-H_2DCFDA staining of ART-treated MDA-MB-468 and SK-BR-3 breast cancer cells after 24 h of culture revealed significant ROS accumulation in comparison to control cells, which was prevented when the ROS scavenger GSH was added at initiation of culture (Fig. 5A). Since ROS accumulation that is in excess of the antioxidant capacity of a cell

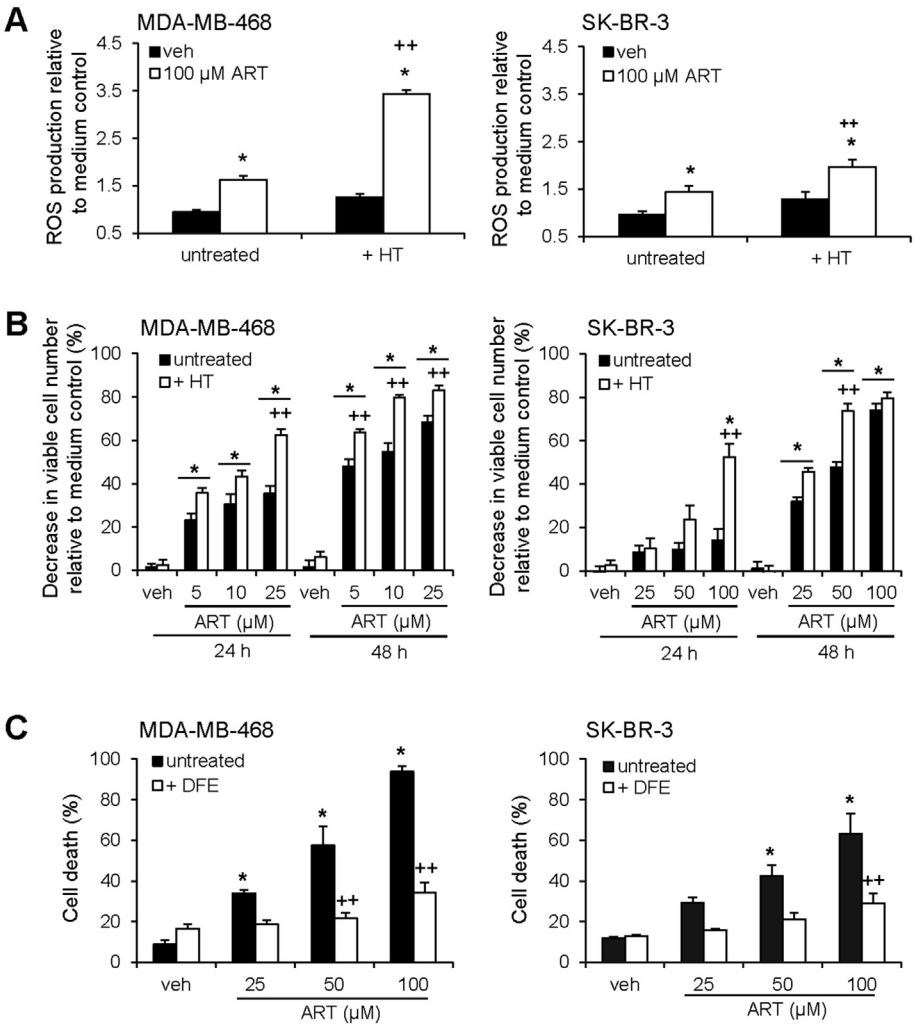

Fig. 7. Evidence that ART-induced ROS accumulation and cytotoxicity involves iron. (A) MDA-MB-468 and SK-BR-3 breast cancer cells were stained with CM-H_2DCFDA prior to treatment with 10 μM HT. Cells were then cultured for 8 h in the presence of 100 μM ART or vehicle (veh) and ROS production was determined by flow cytometry. ART background fluorescence was subtracted from all values. (B) MDA-MB-468 and SK-BR-3 cells were treated with 10 μM HT, then cultured for 24 or 48 h in the presence of the indicated concentrations of ART or vehicle (veh). Cell growth was assessed using an MTT assay. (C) MDA-MB-468 and SK-BR-3 cells were cultured for 48 h in the presence of the indicated concentrations of ART or vehicle (veh) without or with 12.5 μg/ml DFE. Cells were then stained with Annexin-V-FLUOS/PI for flow cytometric analysis. (A, B, C) Data shown are the mean of at least 3 independent experiments ± SEM; * $p < .05$ compared to the vehicle, determined by Student's *t*-test; $^{++}$ $p < .05$ compared to cultures that were not treated with HT or DFE, determined by Student's *t*-test.

causes DNA damage, we determined the impact of ART-induced ROS on the DNA of breast cancer cells by assessing the level of γH2AX, which is a marker of DNA damage (Mah et al., 2010). Both MDA-MB-468 and SK-BR-3 cells showed increased γH2AX following ART treatment (Fig. 5B), which was prevented when GSH was also present. Together, these findings indicate that ART-induced ROS cause DNA damage in breast cancer cells.

We also investigated the impact of ART-induced ROS on the cell cycle, mitochondrial outer membrane permeabilization, and apoptosis induction in cultures of ART-treated breast cancer cells. The anti-proliferative activity of ART was not due to ART-induced ROS accumulation since the addition of GSH at initiation of culture did not rescue cell proliferation (data not shown); however, GSH-mediated ROS scavenging in ART-treated MDA-MB-468 cell cultures caused the percentage of cells in the G1 phase of the cell cycle to increase, along with a corresponding decrease in the G2/M population (Fig. 6A). The percentage of ART-treated SK-BR-3 cells in G1 also increased and the fraction in G2/M decreased in the presence of GSH. These findings suggest a ROS-dependent effect of ART that results in a G2/M arrest and a ROS-independent effect that leads to G1 arrest. ART-induced ROS production was also largely responsible for the loss of mitochondrial outer membrane integrity since the percentage of ART-treated MDA-MB-468 and SK-BR-3 cells with permeabilized mitochondria was dramatically decreased in the presence of GSH (Fig. 6B). It follows that ART-induced ROS accumulation in breast cancer cells contributed to apoptosis induction (Fig. 6C); however, ART-induced cytotoxicity was not completely ablated in the presence of GSH, indicating the involvement of a ROS-independent cytotoxic pathway.

3.5. ART-induced cytotoxicity is iron-dependent

To determine whether ART-induced accumulation of ROS was, at least in part, the result of the iron-catalyzed Fenton reaction (Halliwell, 2001), CM-H_2DCFDA-stained MDA-MB-468 and SK-BR-3 breast cancer cells were loaded with iron in the form of HT prior to culture in the absence or presence of ART. HT-treated cells showed a significant enhancement of ART-induced ROS production (Fig. 7A). Prior exposure to HT also significantly increased the inhibitory effect of ART on the growth of MDA-MB-468 and SK-BR-3 cells (Fig. 7B). In addition, MDA-MB-468 and SK-BR-3 cells that were treated with ART in the presence of iron-chelating DFE exhibited a marked decrease in ART-induced cytotoxicity (Fig. 7C). Taken together, these data indicate that ART-induced ROS production and cytotoxicity in breast cancer cell cultures is iron-dependent.

3.6. ART sensitizes MDA-MB-468 and SK-BR-3 breast cancer cells to chemotherapeutic drugs

To determine whether low-dose ART could sensitize breast cancer cells to chemotherapeutic drugs, MDA-MB-468 cells were exposed to low-dose ART and treated with different concentrations of 4HC (active metabolite of cyclophosphamide), cisplatin, doxorubicin, fluorouracil, or docetaxel. As shown in Fig. 8, combination treatment of MDA-MB-468 cells with low-dose ART resulted in a significant reduction in the

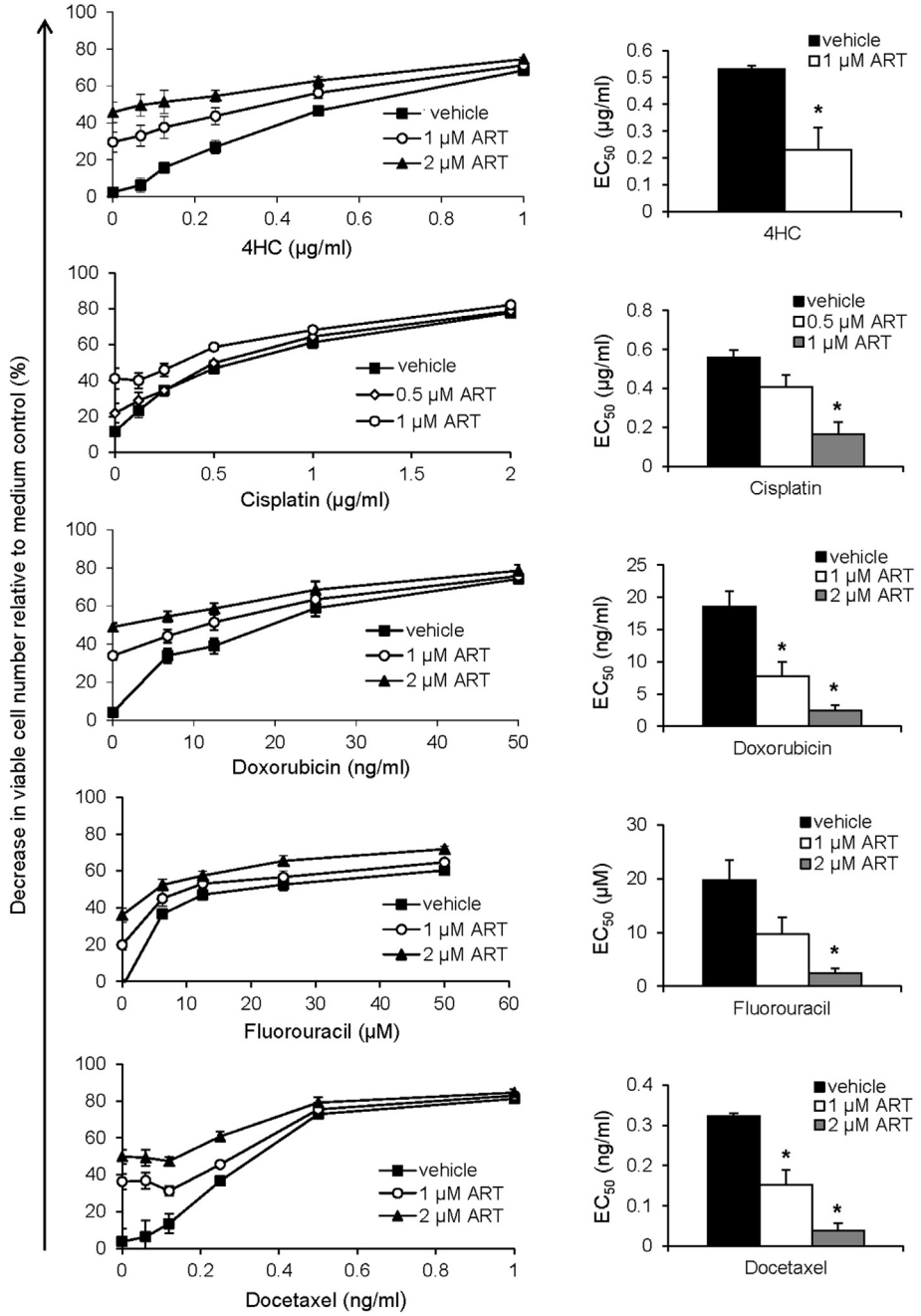

Fig. 8. Chemosensitizing effect of ART on TNBC cells. MDA-MB-468 breast cancer cells were cultured for 72 h with the indicated concentrations of 4HC, cisplatin, doxorubicin, fluorouracil, or docetaxel in the absence or presence of the indicated concentrations of ART or vehicle. Changes in viable cell number were determined using an MTT assay. Data shown are the mean of at least 3 independent experiments ± SEM; *p < .05 compared to EC_{50} of the chemotherapeutic drug alone, determined by a one-way ANOVA with a Tukey-Kramer post-test.

EC_{50} values of all chemotherapeutic agents tested. Prior exposure to low-dose ART also sensitized SK-BR-3 cells to the cytotoxic effect of cisplatin and docetaxel (Supplemental Fig. 4). We also investigated the impact of low-dose ART on the colony-forming capacity of cisplatin-treated MDA-MB-468 cells. Exposure to low-dose ART alone had little effect on colony formation by MDA-MB-468 cells; however, the combination of low-dose ART and cisplatin resulted in a significant reduction in the colony-forming capacity of the breast cancer cells relative the result obtained with cisplatin alone (Fig. 9). Taken together, these data suggest that ART might enhance the effectiveness of chemotherapeutic drugs currently used to treat triple-negative and HER2-enriched breast cancer.

3.7. Hypoxic MDA-MB-468 breast cancer cells resist the cytotoxic effect of ART

Since solid tumors contain areas of hypoxia that promote cancer progression (Nurwidya et al., 2012), we used a hypoxic chamber to study the impact of hypoxia on breast cancer cell killing by ART. As shown in Fig. 10, ART-induced cytotoxicity in MDA-MB-468 cell cultures was markedly reduced after 48 h of culture under hypoxic conditions in comparison to normoxic cultures, i.e., performed in the presence of oxygen. However, MDA-MB-468 cells that were cultured for 24 h under normoxic conditions after treatment with ART, and then placed in a hypoxic environment for an additional 24 h, maintained their sensitivity to ART, suggesting that oxygen must initially be present

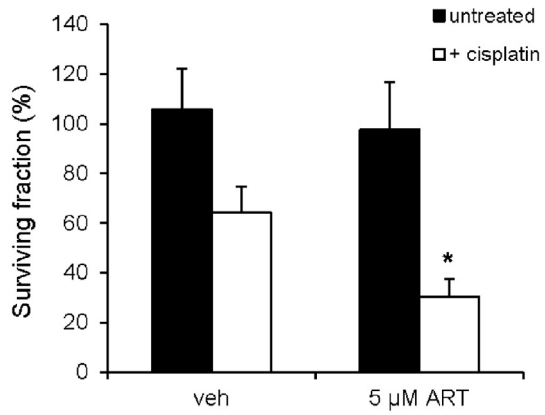

Fig. 9. ART enhances cisplatin-mediated inhibition of colony formation by TNBC cells. MDA-MB-468 breast cancer cells were cultured for 24 h in the absence or presence of 0.1 μM cisplatin without or with 5 μM ART. Equal numbers of viable cells were serially diluted and seeded in triplicate into 6-well plates. Following 14 d culture, colonies were stained with crystal violet and counted. Data shown are the mean of at least 3 independent experiments ± SEM; *p < .05 compared to treatment with cisplatin alone, determined by Student's *t*-test.

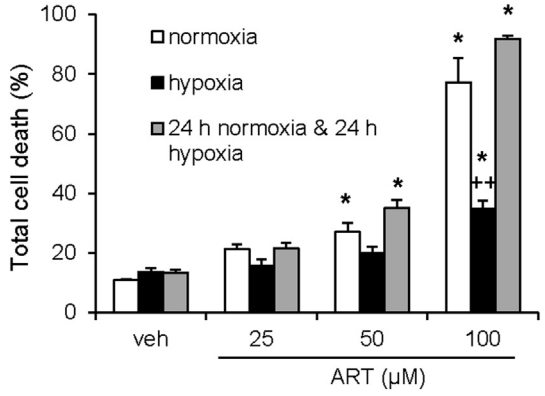

Fig. 10. The cytotoxic effect of ART on TNBC cells is oxygen-dependent. MDA-MB-468 breast cancer cells were treated with the indicated concentrations of ART or vehicle (veh), and then cultured for 48 h in a normoxic or hypoxic environment. Alternatively, ART-treated cells were cultured in a normoxic environment for 24 h and then cultured for another 24 h in a hypoxic environment. At the end of culture, total cell death (early apoptosis plus late apoptosis/necrosis) was determined by flow cytometric analysis of Annexin-V-FLUOS- and PI-stained cells. Data shown are the mean of at least 3 independent experiments ± SEM; *p < .05 compared to the vehicle, $^{++}$ p < .05 compared to normoxic culture, determined by one-way ANOVA with a Tukey-Kramer post-test.

after ART treatment for cell death to take place.

4. Discussion

Previous laboratory studies have investigated the impact of the anti-malarial drug ART and its primary active metabolite dihydroartemisinin on a number of different cancer cell types, including leukemia cells and colorectal, lung, ovarian, and pancreatic carcinoma cells (Efferth et al., 2007; Li et al., 2007; Du et al., 2010; Chen et al., 2013; Greenshields et al., 2017). The present study describes the growth inhibitory effect of ART on 5 different breast cancer cell lines (MDA-MB-468 > T47D > SK-BR-3 > MCF-7 > MDA-MB-231) with differing molecular characteristics, and elucidates the mechanisms that underlie the anti-proliferative and cytotoxic effects of ART on a TNBC cell line (MDA-MB-468) and a HER2-enriched breast cancer cell line (SK-BR-3). Although there was some heterogeneity in sensitivity to ART among the panel of breast cancer cell lines, ART inhibited the growth of all breast cancer cell lines tested, as well as the growth of MCF-10A normal mammary epithelial cells. The inhibitory effect of ART on breast cancer cell growth was also observed in a 3-dimensional culture system (MCF-7), as well as in a colony-forming assay (MDA-MB-468). Importantly, ART inhibited the growth of paclitaxel-resistant MCF-7 breast cancer cells that over-expressed P-glycoprotein, supporting the potential use of ART in the treatment of chemoresistant disease. Altered p53 status did not account for differences in breast cancer cell sensitivity to ART since ER-positive T47D cells with mutant p53 were more sensitive to ART-induced growth inhibition than ER-positive MCF-7 cells with wild-type p53. This is an important finding since p53 is mutated in about 23% of breast cancers and altered p53 correlates with a poor clinical outcome (Walerych et al., 2012).

The anti-proliferative effect of ART on triple-negative MDA-MB-468 and HER2-enriched SK-BR-3 breast cancer cells was the result of cell cycle arrest. The proliferation of MDA-MB-468 cells was arrested in G2/M, whereas SK-BR-3 cells arrested primarily in G1. Both G2/M and G1 cell cycle arrest caused by ART and its metabolite dihydroartemisinin have been reported by investigators working with other cancer cell types. For example, dihydroartemisinin-treated HepG2, PLC/PRF/5 and Hep3B hepatocellular carcinoma cells experience G2/M arrest (Zhang et al., 2012), while ART-treated A431 epidermoid carcinoma cells exhibit G1 arrest (Jiang et al., 2012). An ART-induced non-specific arrest at all phases of the cell cycle has also been reported (Liu et al., 2011). The expression of several key cell cycle regulatory proteins was modulated in ART-treated breast cancer cells. MDA-MB-468 and SK-BR-3 cells that were exposed to ART exhibited decreased expression of CDK1, CDK4, cyclin D3, E2F-1, and CDC25C, as well as increased expression of $p21^{Waf1/Cip1}$. However, some effects of ART were cell line-specific since only SK-BR-3 cells experienced a decrease in cyclin A and cyclin B expression following ART treatment, whereas increased phospho-Chk2 was only observed in ART-treated MDA-MB-468 cells. In line with our findings, ART and dihydroartemisinin-induced cell cycle arrest is associated with altered cell cycle regulatory protein expression by other cancer cell types, including osteosarcoma, gastric, hepatocellular, and epidermoid cancers (Hou et al., 2008; Jiang et al., 2012). Interestingly, subsequent experiments demonstrated that ART-induced ROS accumulation was responsible for G2/M arrest since MDA-MB-468 cells that were exposed to ART in the presence of ROS-scavenging GSH exhibited G1 arrest. ROS-dependent G2/M arrest is also seen in ART-treated HEY ovarian cancer cells (Greenshields et al., 2017). Collectively, these results suggest that ART- and dihydroartemisinin-induced cell cycle arrest of cancer cells is likely cell line and/or tissue-specific, and may be additionally influenced by the artemisinin derivative used, as well as the dosage and timing of treatment.

ART was also directly cytotoxic towards breast cancer cells since both triple-negative MDA-MB-468 and HER2-enriched SK-BR-3 breast cancer cells died by apoptosis following exposure to ART. Importantly, the viability of MCF-10A normal mammary epithelial cells was not affected by ART, which is consistent with the lack of adverse side-effects when ART is used to treat malaria (Rosenthal, 2008). The cytotoxic effect of ART on SK-BR-3 cells was delayed compared to its effect on MDA-MB-468 cells and significant killing of SK-BR-3 cells only occurred after 48 h of culture. Apoptosis of ART-treated MDA-MB-468 and SK-BR-3 breast cancer cells was characterized by the early loss of mitochondrial outer membrane integrity and release of mitochondrial cytochrome *c* and SMAC into the cytosol, which indicates induction of the intrinsic pathway of apoptosis. ART-induced apoptosis of MDA-MB-468 and SK-BR-3 cells was largely caspase-dependent and associated with cleavage of the nuclear DNA-repair protein PARP-1. Increased mitochondrial outer membrane permeability and caspase activation in association with altered Bcl-2 family member expression and/or activation has also been reported in ART- and dihydroartemisinin-treated ER-positive breast cancer cells (Hamacher-Brady et al., 2011; Mao et al., 2013). However, it is apparent that ART activates at least one

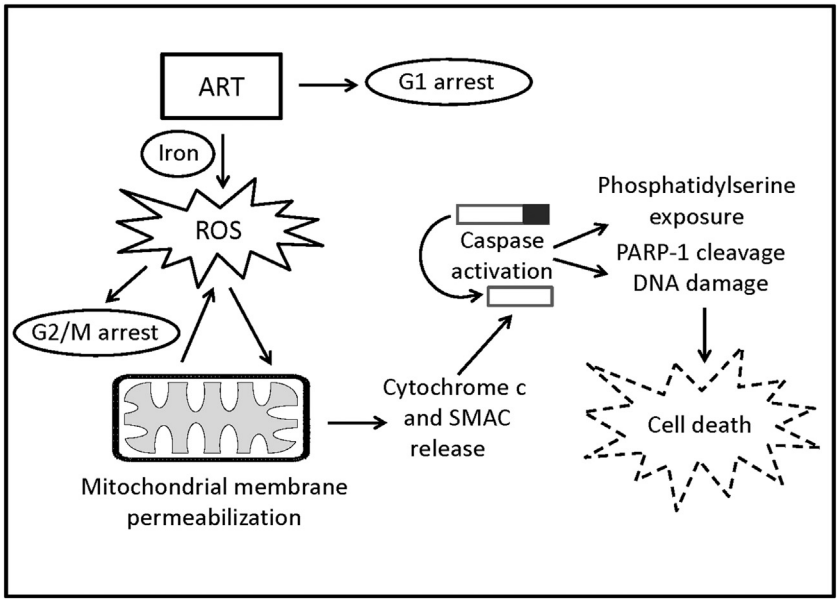

Fig. 11. Scheme for the anti-proliferative and cytotoxic effects of ART in MDA-MB-468 and SK-BR-3 breast cancer cell lines. ART-treated breast cancer cells exhibit ROS-independent G1 phase cell cycle arrest, as well as ROS-dependent G2/M phase cell cycle arrest. Iron-dependent oxidative stress induced by ART also activates the intrinsic pathway of apoptosis, leading to cell death.

other cell death pathway since caspase inhibition failed to reduce the percentage of ART-treated MDA-MB-468 and SK-BR-3 cells undergoing late apoptosis/necrosis. In our hands, ART did not induce necroptosis in MDA-MB-468 and SK-BR-3 breast cancer cells, although ART triggers necroptosis in schwannoma cells (Button et al., 2014). In ovarian cancer cells, exposure to ART results in cell death by ferroptosis (Greenshields et al., 2017), whereas ART-treated pancreatic cancer cells undergo oncosis-like cell death (Du et al., 2010). Oncosis is characterized by cell and organelle swelling, membrane permeability, and cytolysis (Cruchten and Broeck, 2002). Since oncosis-like cell death of ART-treated pancreatic cancer cells involves the loss of mitochondrial outer membrane integrity and is caspase-independent and ROS-dependent (Du et al., 2010), we suggest that oncosis-like cell death may account for the component of caspase-independent cytotoxicity in ART-treated MDA-MB-468 and SK-BR-3 cells.

Intracellular ROS accumulation was important for ART-induced apoptosis of MDA-MB-468 and SK-BR-3 breast cancer cells, as evidenced by the protection afforded by the ROS scavenger GSH against ART-induced DNA damage and cytotoxicity. Interestingly, early ROS accumulation in ART-treated SK-BR-3 cells was less than that observed in ART-treated MDA-MB-468 cells, which may account for differences between SK-BR-3 and MDA-MB-468 cells with respect to their sensitivity to ART. Mitochondrial outer membrane depolarisation induced by ART was also inhibited by GSH, indicating that ROS production occurred upstream of the effect of ART on mitochondria. Our finding that ART-induced ROS production was important for breast cancer cell growth inhibition is consistent with studies in which ART inhibited the growth of other cancer cell types, including leukemia, ovarian cancer, and pancreatic cancer cells, in a ROS-dependent fashion (Efferth et al., 2007; Du et al., 2010; Greenshields et al., 2017). ROS generation and loss of mitochondrial outer membrane integrity was also enhanced in MDA-MB-468 and SK-BR-3 breast cancer cells that were loaded with HT prior to ART treatment, and ART-induced cytotoxicity was diminished in the presence of the iron chelator DFE, implying the involvement of iron in these processes. In this regard, lysosomal iron has been implicated in the killing of MDA-MB-231 and T47D breast cancer cells by ART (Hamacher-Brady et al., 2011). Ferrous iron and/or heme is believed to be necessary for activation of the ART endoperoxide bridge and ROS production (Shandilya et al., 2013). Cancer cells typically maintain higher iron levels than their normal counterparts (Torti and Torti, 2013), which may result in increased sensitivity to ART-induced cytotoxicity. These findings suggest that a transient increase in iron availability within the tumor microenvironment may potentiate the tumoricidal effect of ART in breast cancer patients.

Treatment modalities that combine two or more chemotherapeutic agents are an effective approach to the treatment of triple-negative and HER2-enriched breast cancers (Chalakur-Ramireddy and Pakala, 2018; Escriva-de-Romani et al., 2018). The combination of drugs with different mechanisms of activity, as well as unique toxicity profiles, helps to increase treatment efficacy while limiting adverse side effects and the development of drug resistance. We show here that low doses of ART significantly reduced the EC_{50} values of doxorubicin, cisplatin, docetaxel, fluorouracil and 4HC (active metabolite of cyclophosphamide) for MDA-MB-468 breast cancer cell growth inhibition, revealing an enhancing effect of ART on the in vitro activity of 5 different chemotherapeutic drugs currently used in the treatment of breast cancer (Maughan et al., 2010). A similar enhancing effect of ART treatment on SK-BR-3 sensitivity to cisplatin and docetaxel was also observed. Moreover, a low concentration of ART that by itself was not able to impact the colony-forming capacity of MDA-MB-468 cells significantly reduced the surviving fraction of cisplatin-treated breast cancer cells. This chemosensitizing effect of ART on breast cancer cells is consistent with chemosensitization of other cancer cell types by ART and related compounds (Zhou et al., 2010; Liu et al., 2011). Together, these results support the possible use of ART in combined modality treatments of breast cancer.

Hypoxia is a common feature of solid tumors and is a negative prognostic factor in many cancer types, including breast cancer, because of its metastasis-promoting activity (Nurwidya et al., 2012). Moreover, MDA-MB-231 TNBC cells grown under conditions that mimic the hypoxic tumor microenvironment exhibit increased thioredoxin levels and reduced intracellular ROS production (Karlenius et al., 2012), which would be expected to have a negative effect on ROS-dependent killing of ART-treated breast cancer cells. Indeed, ART-induced cytotoxicity was significantly decreased relative to normoxic controls when MDA-MB-468 cells were exposed to ART under hypoxic conditions, which is consistent with the ROS-dependent cytotoxic effect of ART on both MDA-MB-468 and SK-BR-3 breast cancer cells. Although this finding suggests that cancer cells located in hypoxic regions of a breast tumor may resist killing by ART, hyperbaric oxygen therapy, which is known to improve the effectiveness of ROS-dependent radiotherapy (Stepień et al., 2016), might be used to overcome the inhibitory effect of low oxygen tension on ART-induced cytotoxicity.

5. Conclusion

Fig. 11 depicts a scheme that summarizes the processes that mediate the anti-proliferative and cytotoxic activities of ART against triple-negative and HER2-enriched breast cancer cell lines used in this study. Importantly, ART had no appreciable cytotoxic effect on normal mammary epithelial cells. The multimodal activity of ART on breast cancer cells is an important feature of this drug. The anti-proliferative activity of ART involved intracellular ROS accumulation in that the phase at which cell cycle arrest occurred was dictated by ROS. ART killed breast cancer cells largely via caspase-dependent apoptosis mediated by intracellular ROS accumulation that was promoted by iron. The capacity of ART to sensitize breast cancer cells to chemotherapeutic agents is a particularly important finding that has significant clinical potential; however, in vivo studies showing a therapeutic effect of ART in mouse models of breast cancer are needed to move forward with clinical trials.

Supplementary data to this article can be found online at https://doi.org/10.1016/j.yexmp.2019.01.006.

Conflict of interest

The authors declare that there is no conflict of interest.

Acknowledgement

This study was supported by the Breast Cancer Society of Canada, the Canadian Breast Cancer Foundation and the Queen Elizabeth II Foundation. ALG was the recipient of a Postgraduate Student Award from the Natural Sciences and Engineering Research Council of Canada. DWH is a Senior Scientist of the Beatrice Hunter Cancer Research Institute and holds the Canadian Breast Cancer Foundation-Atlantic Region Endowed Chair in Breast Cancer Research.

References

Brewster, A.M., et al., 2008. Residual risk of breast cancer recurrence 5 years after adjuvant therapy. J. Natl. Cancer Inst. 100, 1179–1183.
Button, R.W., et al., 2014. Artesunate induces necrotic cell death in schwannoma cells. Cell Death Dis. 5, e1466.
Chalakur-Ramireddy, N.K.R., Pakala, S.B., 2018. Combined drug therapeutic strategies for the effective treatment of triple negative breast cancer. Biosci. Rep. 38, BSR20171357.
Chen, T., et al., 2013. Ionizing radiation potentiates dihydroartemisinin-induced apoptosis of A549 cells via a caspase-8-dependent pathway. PLoS One 8, e59827.
Cruchten, S., Broeck, W., 2002. Morphological and biochemical aspects of apoptosis, oncosis and necrosis. Anat. Histol. Embryol. 31, 214–223.
Dai, X., et al., 2015. Breast cancer intrinsic subtype classification, clinical use and future trends. Am. J. Cancer Res. 5, 2929–2943.
Du, J.H., et al., 2010. Artesunate induces oncosis-like cell death in vitro and has antitumor activity against pancreatic cancer xenografts in vivo. Cancer Chemother. Pharmacol. 65, 895–902.
Eckstein, N., 2011. Platinum resistance in breast and ovarian cancer cell lines. J. Exp. Clin. Cancer Res. 30, 91.
Efferth, T., et al., 2007. Artesunate induces ROS-mediated apoptosis in doxorubicin-resistant T leukemia cells. PLoS One 2, e693.
Escriva-de-Romani, S., et al., 2018. HER2-positive breast cancer: current and new therapeutic strategies. Breast 39, 80–88.
Froehlich, K., et al., 2016. Generation of multicellular breat cancer tumor spheroids: comparison of different protocols. J. Mammary Gland Biol. Neoplasia 21, 89–98.
Greenshields, A.L., et al., 2017. Contribution of reactive oxygen species to ovarian cancer cell growth arrest and killing by the anti-malarial drug artesunate. Mol. Carcinog. 56, 75–93.
Halliwell, B., 2001. Free radicals and other reactive species in disease. Encycl. Life Sci. 2001, 1–7.
Hamacher-Brady, A., et al., 2011. Artesunate activates mitochondrial apoptosis in breast cancer cells via iron-catalyzed lysosomal reactive oxygen species production. J. Biol. Chem. 286, 6587–6601.
Ho, W.E., et al., 2014. Artemisinins: Pharmacological actions beyond anti-malarial. Pharmacol. Ther. 142, 126–139.
Hou, J., et al., 2008. Experimental therapy of hepatoma with artemisinin and its derivatives: in vitro and in vivo activity, chemosensitization, and mechanisms of action. Clin. Cancer Res. 14, 5519–5530.
Jiang, Z., et al., 2012. Artesunate induces G0/G1 cell cycle arrest and iron-mediated mitochondrial apoptosis in A431 human epidermoid carcinoma cells. Anti-Cancer Drugs 23, 606–613.
Karlenius, T.C., et al., 2012. Cycling hypoxia up-regulates thioredoxin levels in human MDA-MB-231 breast cancer cells. Biochem. Biophys. Res. Commun. 419, 350–355.
Kayl, A.E., Meyers, C.A., 2006. Side-effects of chemotherapy and quality of life in ovarian and breast cancer patients. Curr. Opin. Obstet. Gynecol. 18, 24–28.
Li, Y., Wu, Y., 2003. An over four millennium story behind qinghaosu (artemisinin)-a fantastic antimalarial drug from a traditional Chinese herb. Curr. Med. Chem. 10, 2197–2230.
Li, L.N., et al., 2007. Artesunate attenuates the growth of human colorectal carcinoma and inhibits hyperactive Wnt/β-catenin pathway. Int. J. Cancer 121, 1360–1365.
Liu, W.M., et al., 2011. The antimalarial agent artesunate possesses anticancer properties that can be enhanced by combination strategies. Int. J. Cancer 128, 1471–1480.
Mah, L.J., et al., 2010. γH2AX: a sensitive molecular marker of DNA damage and repair. Leukemia 24, 679–686.
Mao, H., et al., 2013. Involvement of the mitochondrial pathway and Bim/Bcl-2 balance in dihydroartemisinin-induced apoptosis in human breast cancer in vitro. Int. J. Mol. Med. 31, 213–218.
Maughan, K.L., et al., 2010. Treatment of breast cancer. Am. Fam. Physician 81, 1339–1346.
Murray, S., et al., 2012. Taxane resistance in breast cancer: mechanisms, predictive biomarkers and circumvention strategies. Cancer Treat. Rev. 38, 890–903.
Nurwidya, F., et al., 2012. From tumor hypoxia to cancer progression: the implications of hypoxia-inducible factor-1 expression in cancers. Anat. Cell Biol. 45, 73–78.
Ozben, T., 2007. Oxidative stress and apoptosis : impact on cancer therapy. J. Pharm. Sci. 96, 2181–9216.
Rosenthal, P.J., 2008. Artesunate for the treatment of severe falciparum malaria. N. Engl. J. Med. 358, 1829–1836.
Shandilya, A., et al., 2013. A plausible mechanism for the antimalarial activity of artemisinin: a computational approach. Sci. Rep. 3, 2513.
Siegel, R.L., et al., 2018. Cancer statistics, 2018. CA Cancer J. Clin. 68, 7–30.
Stepień, K., et al., 2016. Hyperbaric oxygen as an adjunctive therapy in treatment of malignancies, including brain tumours. Med. Oncol. 33, 101.
Torti, S.V., Torti, F.M., 2013. Iron and cancer: more ore to be mined. Nat. Rev. Cancer 13, 342–355.
Trachootham, D., et al., 2009. Targeting cancer cells by ROS-mediated mechanisms: a radical therapeutic approach? Nat. Rev. Drug Discov. 8, 579–591.
Valko, M., et al., 2006. Free radicals, metals and antioxidants in oxidative stress-induced cancer. Chem. Biol. Interact. 160, 1–40.
Valko, M., et al., 2007. Free radicals and antioxidants in normal physiological functions and human disease. Int. J. Biochem. Cell Biol. 39, 44–84.
Vellonen, K.S., et al., 2004. Substrates and inhibitors of efflux proteins interfere with the MTT assay in cells and may lead to underestimation of drug toxicity. Eur. J. Pharm. Sci. 23, 181–188.
Walerych, D., et al., 2012. The rebel angel: mutant p53 as the driving oncogene in breast cancer. Carcinogenesis 33, 2007–2017.
Zhang, C.Z., et al., 2012. Dihydroartemisinin exhibits antitumor activity toward hepatocellular carcinoma in vitro and in vivo. Biochem. Pharmacol. 83, 1278–1289.
Zhou, H., et al., 2010. Dihydroartesunateemisinin improves the efficiency of chemotherapeutics in lung carcinomas in vivo and inhibits murine Lewis lung carcinoma cell line growth in vitro. Cancer Chemother. Pharmacol. 66, 21–29.